Opt Quant Electron (2017) 49:71
DOI 10.1007/s11082-017-0901-2

Modelling of hundreds of wavelength long, highly resonant, 3D subwavelength patterned scattering structures

Patrick C. Chaumet[1] · **Anne Sentenac**[1] · **Anne-Laure Fehrembach**[1]

Received: 15 September 2016 / Accepted: 12 January 2017 / Published online: 24 January 2017

Abstract In this paper, we study the performances of the Dipole Discrete Approximation method for modelling the reflectivity of a highly resonant, 3D subwavelength patterned structure extending over tens of thousands wavelength square. The computation time of the whole reflectivity spectrum (80 wavelengths) was about 3 h on a computer and requires about 1.5 GB in memory. These performances make the DDA an unique numerical tool for modelling the scattering by large 3D structures supporting long-range interactions.

Keywords Numerical nodelling · Discrete dipole approximation · Subwavelength scattering structure · Guided mode resonance

1 Introduction

The discrete dipole approximation (DDA), also known as coupled dipole approximation, is a volume integral method based on the Green formalism that was first proposed by Purcell and Pennypacker (1973) for studying the scattering of light by non spherical dielectric

This article is part of the Topical Collection on Optical Wave and Waveguide Theory and Numerical Modelling 2016.

Guest edited by Krzysztof Anders, Xuesong Meng, Gregory Morozov, Sendy Phang, and Mariusz Zdanowicz.

✉ Anne-Laure Fehrembach
anne-laure.fehrembach@fresnel.fr

Patrick C. Chaumet
patrick.chaumet@fresnel.fr

Anne Sentenac
anne.sentenac@fresnel.fr

[1] Aix Marseille Univ, CNRS, Centrale Marseille, Institut Fresnel, F-13013 Marseille, France

grains in free space. In this approach, the objects are defined as a perturbation of a reference medium. The latter is generally a homogeneous medium (Purcell and Pennypacker 1973) but more complex reference media have also been considered, such as multilayers stacks (Rahmani et al. 1997) or even gratings (Chaumet et al. 2003; Chaumet and Sentenac 2009). The main requirement of DDA is to calculate the Green tensor of the reference medium, i.e. it requires the evaluation, at any point, of the field radiated by a dipole placed, at any point, in the reference medium. Once the Green tensor is known, DDA is particularly efficient for simulating the scattering from large inhomogeneous objects as it requires only the meshing of the perturbation.

In this paper, we demonstrate the interest of the DDA by modelling the scattering by a highly resonant non-periodical structure that supports long-wave (hundreds of wavelengths) interactions. We consider a Cavity Resonator Integrated Filter (CRIGF) that is made of a stack of dielectric layers on which is engraved a coupling grating surrounded with two Bragg reflectors (see Fig. 1a). The coupling grating allows the in/out-coupling of an eigenmode of the structure through one diffraction order, leading to a very narrow resonance peak in the diffraction spectrum of the component. The two Bragg reflectors prevent the eigenmode to spread out, thus leading to a high angular tolerance of the resonance. The interest of infinite resonant coupling grating for laser applications and narrow band filtering was suggested more than 30 years ago (Golubenko et al. 1985, 1986; Mashev and Popov 1985). The first theoretical and experimental works on CRIGF demonstrated their interest for laser stabilization (Buet et al. 2012) and narrow band filtering (Kintaka et al. 2012; Buet et al. 2012) with focused beams: resonance peaks with

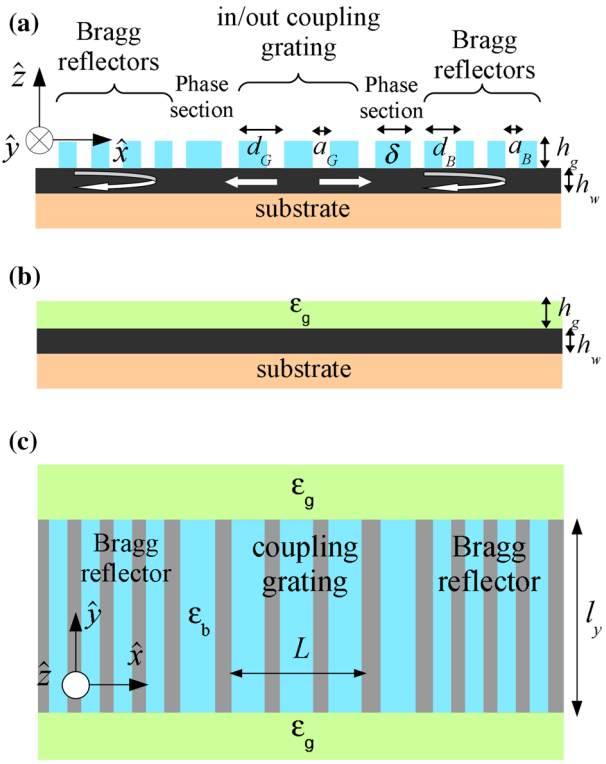

Fig. 1 **a** Geometry of the structure under study (CRIGF). **b** Reference medium that is considered in the DDA. **c** Top view of the modeled structure

spectral width smaller than 1 nm at 850 nm with almost 80 % reflectivity with 11 μm diameter focused incidence beam were obtained. The physic at the basis of the extraordinary properties of CRIGF is under investigation. In particular, the large angular tolerance of CRIGF is attributed to specific mode coupling, which can not occur in infinite gratings (Rassem et al. 2015), that leads to a Fabry–Pérot-like resonance (Laberdesque et al. 2015). The numerical modelling of CRIGF requires a particular care since the structure is hundreds of wavelength long, is extremely resonant, and is structured at the subwavelength scale.

In Chaumet et al. (2016), we performed a successful comparison between four numerical methods (Rigorous Coupled Wave Analysis, Finite Element Method, Finite Difference Time Domain method and the Discrete Dipole Approximation) for simplified CRIGFs which presented one axis of invariance and could be treated as two-dimensional structures. DDA was the only technique that allowed the simulation of the three-dimensional CRIGFs. In this paper, we aim at giving some more details about the implementation of the DDA and provide an analysis of the convergence properties.

2 Structure

The structure under study is represented in Fig. 1. It is made of a central grating, playing the role of an in/out coupling grating, with period $d_G = 480$ nm, holes width $a_G = 240$ nm and number of periods $n_G = 21$. On each side of the central grating, two Bragg reflectors with period $d_B = 240$ nm, holes width $a_B = 120$ nm and number of periods $n_B = 200$ are engraved. The phase section δ is 360 nm. All over the paper, the relative permittivities of the cover and gratings holes are 1, and that of the gratings bumps, waveguiding layer and substrate are respectively ϵ_b=2.13, ϵ_w=3.88 and ϵ_s=2.13. The grating and waveguide thicknesses are respectively $h_g = 120$ nm, and $h_w = 165$ nm. The structure is illuminated from the cover with a Gaussian beam, centered on the central grating, with diameter 10.36μm at waist ($1 / e$ beam diameter for the amplitude, see subsection Incident Gaussian Field, below).

The definition of the reference structure is an important mandatory step when using DDA formulation as it defines the meshing of the object. In this work, we considered different multilayer stacks as reference medium. They are made of the same substrate, cover and waveguiding layer as the structure studied, and the grating layer is replaced with a planar layer with a permittivity ϵ_g (see Fig. 1b). The reference structure is infinite along the x and y directions. Three possibilities for the value ϵ_g will be considered, ϵ_g equal to the relative permittivity of the cover, to the relative permittivity of the grating bumps, or to the geometric mean of the relative permittivity function of the grating.

3 Principle of the computation

3.1 Discrete dipole approximation

The discrete dipole approximation (DDA) was introduced by Purcell and Pennypacker (1973) for studying the scattering of light by non spherical dielectric grains in free space (Purcell and Pennypacker 1973). The object, seen as the perturbation of a reference medium, is represented by a cubic array of N polarizable subunits with a meshsize d over

which the incident and local electric field are assumed to be constant. Under this assumption, the field located at the i-th subunit can be written as:

$$\mathbf{E}(\mathbf{r}_i) = \mathbf{E}^{\text{ref}}(\mathbf{r}_i) + \sum_{j=1}^{N} \mathbf{G}(\mathbf{r}_i, \mathbf{r}_j)\alpha(\mathbf{r}_j)\mathbf{E}(\mathbf{r}_j), \tag{1}$$

where $\mathbf{E}^{\text{ref}}(\mathbf{r}_i)$ denotes the reference field at the position $\mathbf{r}_i$, $\mathbf{G}$ the green tensor (*i.e.* of the reference medium) and $\alpha(\mathbf{r}_j)$ is the polarizability of the subunit j. $\alpha(\mathbf{r}_j)$ is derived from the Clausius–Mossotti expression with the radiative reaction term which is essential to respect the energy conservation (Draine 1988).

$$\alpha_0(\mathbf{r}_j) = \frac{3d^3}{4\pi} \frac{\varepsilon(\mathbf{r}_j) - \varepsilon_m}{\varepsilon(\mathbf{r}_j) + 2\varepsilon_m} \tag{2}$$

$$\alpha(\mathbf{r}_j) = \varepsilon_m \frac{\alpha_0(\mathbf{r}_j)}{1 - \frac{2}{3} ik_m^3 \alpha_0(\mathbf{r}_j)} \tag{3}$$

where ε_m is the permittivity of the reference medium at point $\mathbf{r}_j$ and k_m its wavenumber. Here, the structure is made of isotropic material. Hence, the relative permittivity and subsequently the polarizability are both scalars. The reference field $\mathbf{E}^{\text{ref}}$ represents the field that exists in the reference medium, in absence of the object perturbation, when it is illuminated with the incident field (the reference field contains the incident field).

$\mathbf{G}(\mathbf{r}_i, \mathbf{r}_j)\alpha(\mathbf{r}_j)\mathbf{E}(\mathbf{r}_j)$ represents the field radiated at $\mathbf{r}_i$, by the dipole $\alpha(\mathbf{r}_j)\mathbf{E}(\mathbf{r}_j)$ located at $\mathbf{r}_j$, in presence of the multilayer reference medium, see Fig. 1b. The computation of $\mathbf{G}$ presents some difficulties as the multilayer stack supports guided waves. Indeed, in this case, the Sommerfield integrand, which is used to compute $\mathbf{G}$, exhibits a pole. To obtain an accurate evaluation of the integral without too many integration points, we took an integration path inside the fourth quadrant in the complex plane (Paulus et al. 2000). The method used to perform the quadrature is a Gauss–Kronrod–Patterson method which presents a nested quadrature rule and permits to increase the integration convergence (Patterson 1968). The integration is evaluated with a prescribed accuracy η.

Formally, we derive the field amounts by solving the linear system

$$\mathbf{A}\mathbf{E} = \mathbf{E}^{\text{ref}}, \tag{4}$$

where vectors $\mathbf{E}$ and $\mathbf{E}^{\text{ref}}$ have length $3N$ and contain the induced electromagnetic field and the incident fields, respectively. $\mathbf{A}$ is a matrix of size $3N \times 3N$ which contains the Green function with the polarizabilities. To solve Eq. (4) we use an iterative method called GPBICG which is a refinement of the biconjugate gradient method (Tang et al. 2004), this method is very efficient for the DDA (Chaumet and Rahmani 2009). For a given approximate solution $\mathbf{E}^*$ to Eq. (4), we define the residual as

$$r = \|\mathbf{A}\mathbf{E}^* - \mathbf{E}^{\text{ref}}\| / \|\mathbf{E}^{\text{ref}}\|. \tag{5}$$

The iterative process is terminated once $r < \epsilon$ where ϵ is a prescribed tolerance. Notice that $\mathbf{A}$ has a Toeplitz block structure and then one can use fast Fourier transform to speedup the product $\mathbf{A}\mathbf{E}^*$ in the iterative process (Flatau et al. 1990).

Once, Eq. (1) is solved, the scattered field $\mathbf{E}^{\text{d}}(\mathbf{r})$ at an arbitrary position $\mathbf{r}$ exterior to the object is given by,

$$\mathbf{E}^{\mathrm{d}}(\mathbf{r}) = \sum_{j=1}^{N} \mathbf{G}(\mathbf{r}, \mathbf{r}_j)\alpha(\mathbf{r}_j)\mathbf{E}(\mathbf{r}_j). \tag{6}$$

An analytic expression of $\mathbf{G}$ in presence of the multilayer stack, Belkebir et al. (2005) is used. When $\mathbf{r}$ is in far-field, the sum in Eq. (6) can be performed using a fast Fourier transform (Chaumet et al. 2015).

3.2 Reference Gaussian beam

To specify the reference beam, we introduce the Cartesian basis $(\hat{\mathbf{x}},\hat{\mathbf{y}},\hat{\mathbf{z}})$ where $\hat{\mathbf{z}}$ is the axis normal to the layers, $\hat{\mathbf{x}}$ is the periodicity direction of the gratings and $\hat{}$ indicates normalized vectors. The reference field existing in the reference medium is obtained by shining the multilayer stack with a normally incident $\hat{\mathbf{y}}$-polarized Gaussian beam. We note $\mathbf{e}(\mathbf{k}_{\parallel}, z)\exp(i\mathbf{k}_{\parallel}.\mathbf{r}_{\parallel})$ the field at $\mathbf{r} = \mathbf{r}_{\parallel} + z\hat{\mathbf{z}}$, that is obtained when the multilayer stack is illuminated by a monochromatic plane wave with wavenumber k_0 defined as $\exp(i\mathbf{k}_{\parallel}.\mathbf{r}_{\parallel} - i\gamma z)\hat{\mathbf{s}}(\mathbf{k}_{\parallel})$ where $\gamma = \sqrt{k_0^2 - k_{\parallel}^2}$ and $\hat{\mathbf{s}}$ is the projection of $\hat{\mathbf{y}}$ onto the plane normal to $\mathbf{k}_{\parallel} + \gamma\hat{\mathbf{z}}$. With these definitions, the Gaussian reference field in the multilayer reads,

$$\mathbf{E}^{\mathrm{ref}}(\mathbf{r}) \propto \int_{-k_0}^{k_0}\int_{-k_0}^{k_0} e^{-\frac{k_{\parallel}^2 w_0^2}{2}}\mathbf{e}(\mathbf{k}_{\parallel}, z)e^{i\mathbf{k}_{\parallel}.\mathbf{r}_{\parallel}}\mathrm{d}\mathbf{k}_{\parallel}, \tag{7}$$

where w_0 is the waist of the Gaussian beam. This integral is performed using a Fourier transform.

3.3 Green tensor

Even though we are using an efficient integration scheme to evaluate the Green tensor, it takes a lot of time to evaluate it for all the different pair of points covering the object. Note that due to the translational invariance of the reference medium in the (x, y) plane, $\mathbf{G}(\mathbf{r}, \mathbf{r}') = \mathbf{G}(|\mathbf{r}_{\parallel} - \mathbf{r}'_{\parallel}|, z, z')$. For each couple (z, z'), the number of pairs with different distances of a Cartesian (x, y) mesh with $n_x \times n_y$ points is equal to $n_x(n_x + 1)/2 + (n_x - n_y)n_y$. To accelerate the computation, we approximated $\mathbf{G}(|\mathbf{r}_{\parallel} - \mathbf{r}'_{\parallel}|, z, z')$ using an interpolation of a discrete set of points, $\mathbf{G}(qd/n_d, z, z')$ with $q = 1, \ldots, \mathrm{int}\left(\sqrt{n_x^2 + n_y^2}\right)$ and n_d a natural number. Linear and polynomial interpolations could not evaluate the Green tensor properly when $|\mathbf{r}_{\parallel} - \mathbf{r}'_{\parallel}|/\lambda \ll 1$, as the fast decay of the evanescent waves was not accounted for accurately. We obtained much better results using rational functions, that is quotients of polynomials. Rational functions have the ability to model functions with poles (Press et al. 1986) and permit an accurate approximation of the $1/r^3$ behavior of the Green tensor in the near field range.

4 Results

In this section, we display some convergence studies and computing cost. We evaluate the reflectance spectra of the CGRIF for incident wavelengths varying from 787 to 795 nm.

Otherwise stated, we took $w_0 = 10.36$ µm for the beam waist which corresponds approximately to the beam size maximizing the reflectivity at resonance.

4.1 Study of the convergence of the CGRIF transmission versus the meshsize d and the width l_y

In this paragraph, the permittivity of the reference grating layer is equal to one. Thus, the structure should be seen as a multilayer on which are deposited small prisms of glass in a limited area. The reflection spectra is calculated for different meshsize ($d = 120$ nm, $d = 60$ nm and $d = 40$ nm) and different widths ($l_y = 21d_G$, $l_y = 31d_G$, $l_y = 42d_G$) of the structure along the y direction. We use as reference result the one obtained with the smallest mesh size $d = 40$ nm and the biggest width $l_y = 42d_G$. In Fig. 2, we observe that the position and shape of the resonance are accurately determined when $d = 60$ nm and for a width about $31d_G$.

To confirm this result, we consider a structure with $42d_G$-width and we plot the ratio of the reflected plus the transmitted flux of the Poynting vector over the incident flux versus the meshsize in Fig. 3. Note that the latter is not theoretically equal to one, even though the materials are lossless, as some energy may be taken away by the guided wave if the uncoupling is not complete (leakage of the guide mode through the Bragg grating). However, for $d = 60$ nm the ratio is close to 1 at 0.6% and for $d = 40$ nm it is close to 1 at 0.1%. Then we can conclude that the meshsize $d = 60$ nm is a good compromise between precision and time of computation.

4.2 Influence of the permittivity of the reference grating layer

In this paragraph, we study the influence of the reference grating layer permittivity on the convergence of the simulations. In a first study, we considered a homogenized value for the permittivity of the reference layer, $\varepsilon_g = \varepsilon_h = (\varepsilon_b + 1)/2$, Fig. 4. In this case, the structure matches that studied in the previous paragraph only in the grating area (see Fig. 1c) and it cannot be obtained experimentally. In a second study, we took the permittivity of the grating as reference value, $\varepsilon_g = \varepsilon_b$. In this case, the structuration can be obtained by drilling holes into glass layer, Fig. 5. Once again, this configuration matches that studied in the previous paragraph only in the grating area. However, despite the geometrical

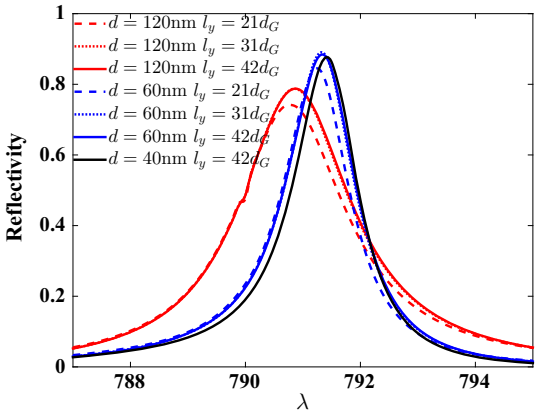

Fig. 2 Reflectance spectra for several values of the meshsize and width of the CRIGF

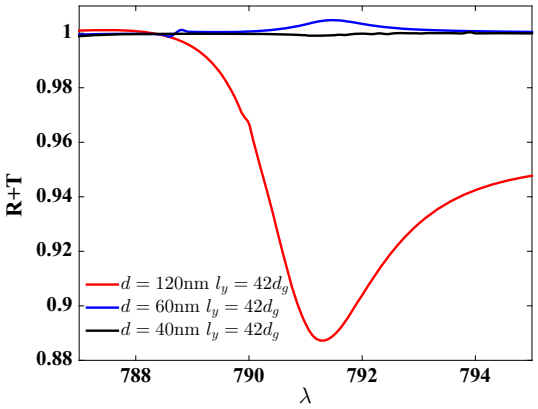

Fig. 3 Ratio of the reflected plus the transmitted flux of the Poynting vector over the incident flux

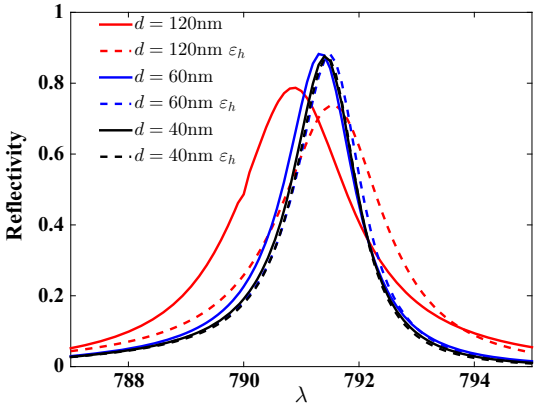

Fig. 4 Reflection spectrum for several value of the mesh size when the reference grating layer permittivity is the homogenized permittivity

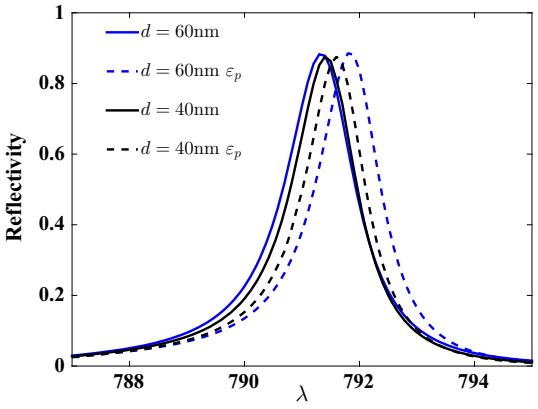

Fig. 5 Reflection spectrum for several value of the mesh size when the reference grating layer permittivity is that of the grating bumps

differences between these configurations, they should yield the same result as the incident beam is focused onto the center of the grating and the total field decays rapidly at the edges of the structured area. It is observed in Fig. 4 that the homogenized permittivity permits a

faster convergence of the simulation as the spectrum obtained for 120 nm is significantly more accurate (considering the centering wavelength of the peak) than that obtained when the permittivity ε_g is one. This behavior can be explained by the fact that the mode of the reference medium is closer to that of the actual structure so that the perturbation permittivity contrast on the resonance wavelength is smaller. On the other hand, taking a reference permittivity equal to that of the grating bumps is clearly not a good solution as the convergence is slower (see Fig. 5). Indeed, taking a reference medium with high permittivity implies a faster oscillating Green tensor so that the assumption that it must be constant within one subunit is more difficult to satisfy.

4.3 Computation time and memory requirements

In this last paragraph we investigate the computation time and the memory that are required to deal with these large objects.

When the meshsize is decreased from 120 to 60 (40) nanometers, the number of unknowns N is increased by a factor of 8 (27). We observe in Table 1 that, surprisingly, the computation time increases less than the increase of unknowns. Now, the most time consuming step in the algorithm is the iterative solving of the linear system (with prescribed accuracy ϵ) which is usually said to depend on $N \log N$. Actually, this indication is not precise enough : the inversion time depends also on the number of iterations. Keeping the same number of unknowns, if the initial guess is close to the solution, the inversion will be much faster than if the initial guess is far from the actual solution. In Fig. 6 we plot the number of iterations versus the wavelength for different meshsize. In these calculations, the initial guess at a given wavelength is the solution obtained for the previous wavelength (Chaumet et al. 2008). For the first wavelength, the initial guess is the Born solution (replacing E by E_{ref} in the right hand side of Eq. 4). We observe that the number of iterations is roughly the same whatever the wavelength for the meshsize 60 and 40 nm while it varies with huge peaks for coarsest meshsize. Note that an iteration number about 2000 indicates that the inversion could not be obtained within the prescribed accuracy. A possible explanation of the high number of iterations that is necessary with the 120 nm meshing is that the field change from one subunit to its closest neighbour is more important than the change obtained with 60 and 40 nm meshsize. This rapidly oscillating solution is more difficult to obtain. This analysis shows that increasing the meshsize in order to diminish the number of unknowns has to be done with caution. It also points out that, when the meshsize is appropriate, there is no additional difficulty when the structure resonates. We have also studied the computation time when the width l_y is increased for a fixed meshsize of 120 nm, see Table 2. Unsurprisingly, in this case the computation time increases linearly with the number of unknowns (with the widths).

Last, we investigated the role of the inversion and Green tensor accuracies for a meshsize $d = 60$ nm and $l_y = 42 d_G$ on the position of the resonance. We observed that ϵ

Table 1 Computation time of the reflection spectrum (80 wavelengths from 787 to 795 nm) obtained with a prescribed accuracy of $\eta = \epsilon = 10^{-5}$, $l_y = 42 d_G$ versus the meshsize d and memory needs for the computer

Meshsize (nm)	120	60	40
Computation time (s)	9400	47400	172000
Memory (GB)	1.3	4.5	13.5

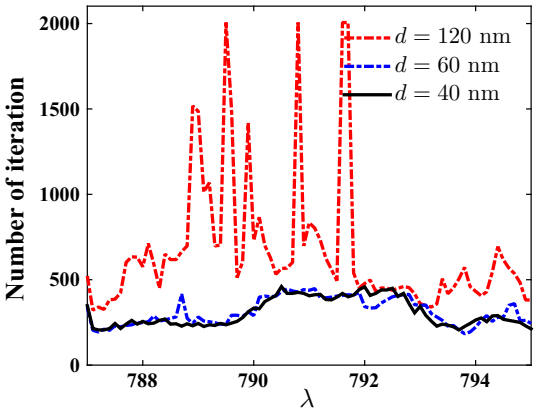

Fig. 6 Number of iterations required by the inversion scheme to obtain an accuracy $\epsilon = 10^{-5}$ versus the wavelength for different meshsize with $l_y = 42d_G$

Table 2 Computation time of the reflectivity spectrum with an accuracy of $\eta = \epsilon = 10^{-5}$, d =120 nm versus l_y

l_y	$21d_G$	$31d_G$	$42d_G$
Computation time (s)	4300	6300	9400

Table 3 Magnitude of the resonance of the Green tensor (guided mode) and computation time for $d = 60$ nm, $l_y = 42d_G$ at $\lambda = 791.3$ nm, $\eta = 10^{-5}$ versus the number of subpixels points taken in the Green tensor interpolation n_d

n_d	1	2	3	4	Rigorous
Magnitude of the resonance	0.4544	0.8825	0.8793	0.8795	0.8795
Time of computation (s)	16	33	49	66	37403

The 'rigorous' row corresponds to calculations performed without interpolating the Green tensor

should be smaller than 10^{-3} and that the integration of the Green tensor should be performed within an accuracy of $\eta = 10^{-4}$ at least. The interpolation is based on a four points rational function with n_d equal to 2 at least, see Table 3.

5 Conclusion

In conclusion, we have shown that the Dipole Discrete Approximation method is able to simulate the diffraction by large highly resonant objects. We have studied the role of the meshsize, reference medium, tolerance of the inversion and accuracy of the Green tensor on the convergence of the simulation. We have observed that, with the appropriate parameters, the computation time of the whole reflectivity spectrum (80 wavelengths) is about 3 h on a computer and requires about 1.5 GB in memory for the lowest

discretization. These performances make DDA the most efficient numerical technique, to date, for simulating the far-field diffraction by large three-dimensional complex structures.

Acknowledgements This work benefited from the financial support from Agence Nationale de la Recherche and Direction Générale de l'Armement, Astrid program (CALITREC project).

References

Belkebir, K., Chaumet, P.C., Sentenac, A.: Superresolution in total internal reflection tomography. J. Opt. Soc. Am. A **22**, 1889–1897 (2005)

Buet, X., Guelmani, A., Monmayrant, A., Calvez, A., Tourte, C., Lozes-Dupuy, F., Gauthier-Lafaye, O.: Wavelength-stabilised external-cavity laser diode using cavity resonator integrated guided mode filter. Electron. Lett. **48**, 1619–1621 (2012a)

Buet, X., Daran, E., Belharet, D., Lozes-Dupuy, F., Monmayrant, A., Gauthier-Lafaye, O.: High angular tolerance and reflectivity with narrow bandwidth cavity-resonator-integrated guided-mode resonance filter. Opt. Express **20**, 9322–9327 (2012b)

Chaumet, P.C., Rahmani, A.: Efficient iterative solution of the discrete dipole approximation for magnetodielectric scatterers. Opt. Lett. **34**, 917–919 (2009)

Chaumet, P.C., Sentenac, A.: Simulation of light scattering by multilayer cross-gratings with the coupled dipole method. J. Quant. Spect. Rad. Transf. **110**, 409–414 (2009)

Chaumet, P.C., Rahmani, A., Bryant, G.W.: Generalization of the coupled dipole method to periodic structures. Phys. Rev. B **67**, 165404–165405 (2003)

Chaumet, P.C., Belkebir, K., Rahmani, A.: Coupled-dipole method in time domain. Opt. Express **16**, 20157–20165 (2008)

Chaumet, P.C., Zhang, T., Sentenac, A.: Fast far-field calculation in the discrete dipole approximation. J. Quant. Spectrosc. Radiat. Transf. **165**, 88–92 (2015). ISSN 0022-4073

Chaumet, P.C., Demésy, G., Gauthier-Lafaye, O., Sentenac, A., Popov, E., Fehrembach, A.-L.: Electromagnetic modeling of large subwavelength-patterned highly resonant structures. Opt. Lett. **41**, 2358–2361 (2016)

Draine, B.T.: The discrete-dipole approximation and its application to interstellar graphite grains. Astrophys. J. **333**, 848–872 (1988)

Flatau, P.J., Stephens, G.L., Draine, B.T.: Light scattering by rectangular solids in the discrete-dipole approximation: a new algorithm exploiting the Block-Toeplitz structure. J. Opt. Soc. Am. A **7**, 593–600 (1990)

Golubenko, G., Svakhin, A., Sychugov, V., Tischenko, A.: Total reflection of light from a corrugated surface of a dielectric waveguide. Sov. J. Quantum. Electron. **15**, 886–887 (1985)

Golubenko, G., Svakhin, A., Sychugov, V., Tischenko, A., Popov, E., Mashev, L.: Diffraction characteristics of planar corrugated waveguides. Opt. Quantum. Electron. **18**, 123–128 (1986)

Kintaka, K., Majima, T., Inoue, J., Hatanaka, K., Junji, N., Ura, S.: Cavity-resonator-integrated guided-mode resonance filter for aperture miniaturization. Opt. Express **20**, 1444–1449 (2012)

Laberdesque, R., Gauthier-Lafaye, O., Camon, H., Monmayrant, A., Petit, M., Demichel, O., Cluzel, B.: High-order modes in cavity-resonator-integrated guided-mode resonance filters (CRIGFs). J. Opt. Soc. Am. A **32**, 1973–1981 (2015)

Mashev, L., Popov, E.: Zero order anomaly of dielectric coated gratings. Opt. Commun. **55**, 377–380 (1985)

Patterson, T.N.L.: The optimum addition of points to quadrature formulae. Math. Comput. **22**, 847–856 (1968)

Paulus, M., Gay-Balmaz, P., Martin, O.J.F.: Accurate and efficient computation of the Green's tensor for stratified media. Phys. Rev. E **62**, 5797–807 (2000)

Press, W.H., Flannery, B.P., Teukolski, S.A., Vetterling, W.T.: Numerical Recipes. The Art of Scientific Computing. Cambridge University Press, Cambridge (1986)

Purcell, E.M., Pennypacker, C.R.: Scattering and absorption of light by nonspherical dielectric grains. Astrophys. J. **186**, 705–714 (1973)

Rahmani, A., Chaumet, P.C., de Fornel, F., Girard, C.: Field propagator of a dressed junction: fluorescence lifetime calculations in a confined geometry. Phys. Rev. A **56**, 3245–3254 (1997)

Rassem, N., Fehrembach, A.-L., Popov, E.: Waveguide mode in the box with an extraordinary flat dispersion curve. J. Opt. Soc. Am. A **32**, 420–430 (2015)

Tang, J., Shen, Y., Zheng, Y., Qiu, D.: An efficient and flexible computational model for solving the mild slope equation. Coast. Eng. **51**, 143–154 (2004)